

# Spintronic properties and stability of the half-Heusler alloys LiMnZ (Z=N, P, Si)

L. Damewood,<sup>1</sup> B. Busemeyer,<sup>2</sup> M. Shaughnessy,<sup>3</sup> C. Y. Fong,<sup>1</sup> L. H. Yang,<sup>4</sup> and C. Felser<sup>5</sup>

<sup>1</sup>*Department of Physics, University of California, Davis, CA 95616 USA\**

<sup>2</sup>*Department of Physics, University of Illinois, Urbana, IL 61801 USA*

<sup>3</sup>*RTBiQ, Inc., San Francisco, CA 94121 USA*

<sup>4</sup>*Lawrence Livermore National Laboratory, Livermore, CA 94551 USA*

<sup>5</sup>*Institut für Anorganische Chemie und Analytische Chemie,  
Johannes Gutenberg-Universität Mainz, 55099 Mainz, Germany*

(Dated: November 5, 2014)

Li-based half-Heusler alloys have attracted much attention due to their potential applications in optoelectronics and because they carry the possibility of exhibiting large magnetic moments for spintronic applications. Due to their similarities to metastable zinc blende half-metals, the half-Heusler alloys  $\beta$ -LiMnZ (Z = N, P and Si) were systematically examined for their electric, magnetic and stability properties at optimized lattice constants and strained lattice constants that exhibit half-metallic properties. Other phases of the half-Heusler structure ( $\alpha$  and  $\gamma$ ) are also reported here, but they are unlikely to be grown. The magnetic moments of these stable Li-based alloys are expected to reach as high as  $4 \mu_B$  per unit cell when Z = Si and  $5 \mu_B$  per unit cell when Z = N and P, however the antiferromagnetic spin configuration is energetically favored when Z is a pnictogen.  $\beta$ -LiMnSi at a lattice constant 14% larger than its equilibrium lattice constant is a promising half-metal for spintronic applications due to its large magnetic moment and vibrational stability. The modified Slater–Pauling rule for these alloys is determined. Finally, a plausible method for developing half-metallic  $\text{Li}_x\text{MnZ}$  at equilibrium, by tuning  $x$ , is investigated, but, unlike tetragonalization, this type of alloying introduces local structural changes that destroy the half-metallicity.

Keywords: half-Heusler alloys, half-metals, antiferromagnetic

## I. INTRODUCTION

Ternary compounds involving the Li atom in the form of half-Heusler, or semi-Heusler, alloys, have recently attracted attention because of their potential in optoelectronic and spintronic applications[1, 2]. The crystal structure,  $C1_b$ , of any half-Heusler alloy is similar to the structure,  $L2_1$ , of a full-Heusler alloy ( $X_2YZ$ ) but missing one X. Due to the missing element, these alloys have three distinct atomic arrangements, called  $\alpha$ -,  $\beta$ - and  $\gamma$ -phases[3], used by various research groups [1–7]. In **Table I**, the positions occupied by the three atoms and the vacancy are given according to the notations defined by Wyckoff [8]. One of the authors (C. F.)[1] examined lithiated half-Heusler alloys in the  $\beta$ -phase, namely LiMgZ (Z = N, P, As, Bi), LiYP, LiY (Y = Zn, Cd) and LiAlSi. They found that covalent bonding between the Y and Z atoms forms the gap of these compounds. They suggested these half-Heusler alloys could be used in optoelectronic and solar applications because the values of the band gaps and lattice constants of these materials are suitable for substituting CdS as buffer layer materials. Since there is no magnetic element in any of these alloys, magnetic properties were not addressed. Jungwirth *et al.* [2] considered a magnetic element in a Li-based half-Heusler alloy and epitaxially grew  $\beta$ -LiMnAs on an InAs substrate. They theoretically predicted that  $\beta$ -LiMnAs is antiferromagnetic and confirmed it experimentally using a SQUID to measure the magnetic moment.

TABLE I. The positions of the three atoms, X, Y and Z in terms of the Wyckoff notation:  $4a = (0,0,0)a$ ,  $4b = (1/2,1/2,1/2)a$ , and  $4c = (1/4,1/4,1/4)a$ , where  $a$  is the lattice parameter. The zinc blende structure, YZ, is included for comparison.

Structure	X	Y	Z
$\alpha$	4c	4b	4a
$\beta$	4b	4a	4c
$\gamma$	4a	4c	4b
Zinc blende	–	4a	4c

The studies of transition metal element (TME)-based half-Heusler alloys indicate that there are a number of differences among the three phases. Using the  $\alpha$ -phase for TME-based half-Heusler alloys (X=Fe, Co, Ni; Y=Ti, V, Zr, Nb, Mn), Tobola and Pierre [7] and Galanakis *et al.* [6] showed that the d–d bonding between X and Y, of the half-metal (HM) CrMnSb, is responsible for the states at the gap in the insulating channel. A HM exhibits metallic properties in one spin channel and semiconducting properties in the oppositely oriented spin channel. They did not comment on the d–p bonding states between X and Z. We previously suggested[9] a point of view in Heusler alloys unifying the d–p and the d–d bonding: Z is the most electronegative among the three atoms so it should form d–p bonding and determine the primary bonding properties of the bonding–antibonding gap. Additionally, the weak bonds between the two TM atoms, formed by d–d bonding, contribute to the states at the gap. From this

\* damewood@physics.ucdavis.edu

point of view, the TME-based half-Heusler alloys, such as CrMnSb, in  $\alpha$ - and  $\gamma$ -phases, differ by which of the two TM atoms is the nearest neighbor (nn) of Z. Their properties differ accordingly.

How does our suggestion, *to consider the nn of Z*, work for Li-related half-Heusler alloys? We expect that the  $\beta$ -phase is energetically favored because Z, the most electronegative element, is nn to both Li and Mn. We also anticipate a larger gap than the TME-based half-Heusler alloys since there is no d-d bonding forming states in the gap. Based on the fact that Li easily gives up its outermost electron to its neighbor,  $\beta$ -LiMnZ can be viewed as an intercalation of zinc blende  $(\text{MnZ})^-$  and  $\text{Li}^+$ [1]. According the ionic model[10], Mn loses three valence electrons to the pnictogen Z when they are nn pairs, and the four remaining d-electrons combine with the electron from Li to give a local magnetic moment as large as  $5 \mu_B$  per Mn. If Z is a group IV element, then the maximum is  $4 \mu_B$  per Mn.

Typical TME-based zinc blende alloys, such as MnZ, are not half-metallic at their equilibrium lattice constant. The standard method to obtain half-metallic properties from these alloys is to increase, or shrink, their lattice constant by growing them as thin films on substrates with larger, or smaller, lattice constants[11]. Straining the lattice constant of the alloy can manifest half-metallic properties by changing the bonding and exchange strength between atoms[12]. These changes can shift the Fermi energy into a gap of one spin channel while the Fermi energy cuts through states in the other spin channel, resulting in a HM. We examine the alloys for large magnetic moments or even half-metallic properties at lattice constants away from equilibrium.

Since Li-based alloys, other than the ones included in this report, may be desirable to grow, we determined the modified Slater-Pauling (SP) rule[13] for Li-based half-Heusler alloys based on the band structure calculations. The rule provides a zeroth order approximation to the magnetic moment of ferromagnets based on the number of occupied states in the minority spin channel  $N_\downarrow$ . Combined with the fact that the total number of valence states is  $N = N_\downarrow + N_\uparrow$ , the magnetic moment is

$$M = N_\downarrow - N_\uparrow = N - 2N_\downarrow \quad (1)$$

in units of  $\mu_B$ . The modified SP rule is useful for predicting the magnetic moment of materials where  $N_\downarrow$  may remain constant, but N changes by replacing atoms with neighboring atoms on the periodic table. The As mentioned previously, Jungwirth *et al.* [2] already determined that  $\beta$ -LiMnAs favors the antiferromagnetic configuration, so we examined the possibility that ferromagnetism is energetically favored over antiferromagnetism in any of the alloys.

For these alloys to be useful in devices, the issue of stability should be addressed. In the past, the conventional wisdom is that the thin film forms of HMs with lattice constants away from the equilibrium values are

stable up to  $\sim 100$  layers[11], but we question this claim. We compared the stability of  $\beta$ -LiMnP to meta-stable ZB MnP, by considering phonon spectra determined by the response function method[14].

With the Li-based alloys, it seems plausible to shift the Fermi energy  $E_F$  by adjusting the concentration of Li atoms. For an alloy where its  $E_F$  cuts through the bottom of the conduction band of one spin channel, will lowering the concentration of Li push the Fermi energy into the gap and give a HM at equilibrium? We use the location of  $E_F$  with respect to the gap as a guide to investigate the possibility of half-metallicity in  $\text{Li}_x\text{MnZ}$  alloys, with  $x < 1$ .

In this paper, we investigate three LiMnZ with  $Z = \text{N}, \text{P}$  and  $\text{Si}$  and address the following issues:

- What are the basic bonding and magnetic properties of LiMnZ, particularly in the lowest energy phase?
- Compared to zinc blende MnZ, what is the role of Li in the electronic and magnetic properties of LiMnZ?
- Can any of the alloys energetically favor the ferromagnetic phase and give a large magnetic moment?
- How does the phonon stability of  $\beta$ -LiMnZ compare to ZB MnZ and what are the implications for growth?
- Finally, can adjusting the concentration of Li in  $\beta$ - $\text{Li}_x\text{MnZ}$  result in a HM at equilibrium?

In [Section II](#), we discuss the models used to answer these questions, and present a brief description of the methods of calculation. Results and discussion of the above issues will be presented in [Section III](#). Finally, in [Section IV](#), we summarize our findings.

## II. STRUCTURAL MODELS AND METHODS OF CALCULATION

We used the primitive cell to find the equilibrium lattice constants by means of minimizing the total energy of each alloy with respect to the lattice constant. The phonon calculations also rely on the respective primitive cells of  $\beta$ -LiMnP and ZB MnP. We calculate the antiferromagnetic properties by constructing a tetragonal cell, consisting of two formula units of LiMnZ, to allow the possibility of antiparallel alignment of Mn atoms. Additionally, we explored the possibility of lower concentrations of Li atoms by constructing conventional unit cells consisting of four formula units of LiMnZ and then removing one Li atom and letting the atoms and unit cell relax to equilibrium. The resulting alloys are denoted  $\text{Li}_3\text{Mn}_4\text{Z}_4$ , or  $\text{Li}_{0.75}\text{MnZ}$ .

We used the spin-polarized version of the VASP code[15–18], which is based on density functional theory (DFT)[19]. The generalized gradient approximation

(GGA) of Perdew *et al.* [20] (PBE) was used to treat the exchange-correlation between electrons. GGA provides realistic bonding and magnetic properties, except for the value of the semiconducting gap. The value of the semiconducting gap is not a crucial issue at this point, so we did not consider more complicated methods utilizing many-body techniques. Many-body methods improve upon the conduction states in semiconductors and HMs[21], but also show that half-metallic properties may disappear at finite temperatures[22].

The VASP package provides projector-augmented-wave (PAW) pseudopotentials[23] for Li, Mn, N, P, and Si that were constructed using PBE. We used a basis of plane waves with a 1000 eV kinetic energy cutoff for all calculations. The Monkhorst–Pack[24] meshes of (17,17,17), (15,15,15) and (11,11,11) were adopted for the Brillouin Zone (BZ) of the primitive, tetragonal and the conventional cells, respectively. Using these values, the convergence of the total energy and the magnetic moment of any sample are better than 1.0 meV and 1.0  $\mu_B$ , respectively.

To address the stability of the lithiated compounds, we used the ABINIT software package to perform response-function phonon calculations[25, 26]. We used the same exchange-correlation functional as in VASP and used comparable convergence parameters to calculate the ground state structure. To calculate the force constants, a 4x4x4 irreducible  $\vec{q}$ -point grid, centered at  $\vec{q} = (0, 0, 0)$  was constructed.

### III. RESULTS AND DISCUSSION

#### A. Basic Properties of LiMnZ

Using the primitive unit cell, we first determined the equilibrium lattice constants of the three compounds in the three phases ( $\alpha$ -,  $\beta$ - and  $\gamma$ -phases). The results are summarized in Table II. The lattice constants correlate with the covalent radii of Z ( $r_{\text{cov}}(\text{N}) = 0.71 \text{ \AA}$ ,  $r_{\text{cov}}(\text{P}) = 1.09 \text{ \AA}$ , and  $r_{\text{cov}}(\text{Si}) = 1.14 \text{ \AA}$ [27]. The  $\beta$ -phase is consistently the lowest energy phase because Z, the most electronegative element, is nn to both Mn and Li.

In Fig. 1, we show the density of states (DOS) for  $\alpha$ - and  $\beta$ -LiMnSi with partial DOS of the so-called  $e_g$  (doubly degenerate  $d_{z^2}$  and  $d_{x^2-y^2}$ ) and  $t_{2g}$  (triply degenerate  $d_{xy}$ ,  $d_{yz}$ , and  $d_{zx}$ ) states. Here, we choose to only discuss the bonding properties of LiMnSi since, at the equilibrium lattice constant, the overall bonding features are not significantly altered when Z = N or P. The  $\beta$ - and  $\gamma$ -phase DOSs are very similar—both have Mn and Si as nn and the position of the Li atom does not drastically alter the DOS—so the  $\gamma$ -phase is not included. The  $\beta$ - and  $\gamma$ -phases form a large bonding–antibonding gap, due to the overlap of the  $t_{2g}$  states of Mn and Si  $sp^3$  states in the tetrahedral environment. The  $\alpha$ -phase is significantly different compared to the  $\beta$ - and  $\gamma$ -phases and does not form a large bonding–antibonding gap because the Mn

TABLE II. The equilibrium lattice constants, total energies, and magnetic moments for three lithiated half-Heusler alloys.

Compound	Lattice constant ( $\text{\AA}$ )	Total energy relative to $\beta$ (eV)	Magnetic moment ( $\mu_B/\text{Mn}$ )
$\alpha$ -LiMnN	4.961	2.379	4.675
$\beta$ -LiMnN	4.912	0.000	3.925
$\gamma$ -LiMnN	5.139	1.992	4.805
$\alpha$ -LiMnP	5.600	1.218	4.391
$\beta$ -LiMnP	5.717	0.000	4.090
$\gamma$ -LiMnP	5.715	0.661	3.987
$\alpha$ -LiMnSi	5.629	0.721	3.750
$\beta$ -LiMnSi	5.778	0.000	3.314
$\gamma$ -LiMnSi	5.788	0.395	3.301

and Si are second neighbors in a cubic environment.

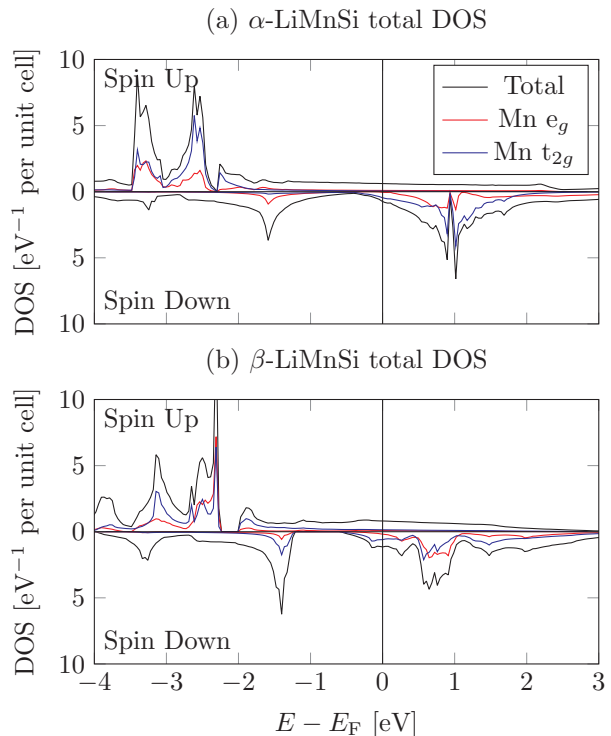


FIG. 1. Spin polarized total density of states (DOS) for LiMnSi in (a)  $\alpha$ - and (b)  $\beta$ -phases at their respective equilibrium lattice constants. The Mn  $e_g$  and  $t_{2g}$  partial DOS are shown as the shaded areas.

#### B. The role of Li in LiMnZ

We have argued that Li easily gives up its valence electron to its nearest neighbor. To substantiate this argument, we compare  $\beta$ -LiMnSi to MnSi in the ZB structure.

The latter is predicted to be a HM in which the bonding, antibonding and non-bonding states are easily identified [12]. In Fig. 2, we compare the states around  $E_F$  at  $\Gamma$  of the two spin channels for  $\beta$ -LiMnSi and MnSi at the same lattice constant of 5.778 Å, and show the size of the bonding–antibonding gap (the energy difference between the top of the valence band and the bottom of the conduction band, in the minority spin channel, at the  $\Gamma$ -point). The primary effects of Li are: (1) increasing the width of the occupied states and (2) promoting its s-state to the p-states and contributing to the d–p mixed states. The second effect indicates that Li gives up its electron. The argument that the Li is giving up its electron is also reflected in the charge density difference,  $\beta$ -LiMnSi minus MnP, shown in Fig. 3. This plot shows the Li electron redistributes its charge to Mn (i) and Si (ii), away from Li, and causes the d–p hybridized bond between Mn and P to weaken, thereby shifting the bond charge away from P and towards Mn (iii).

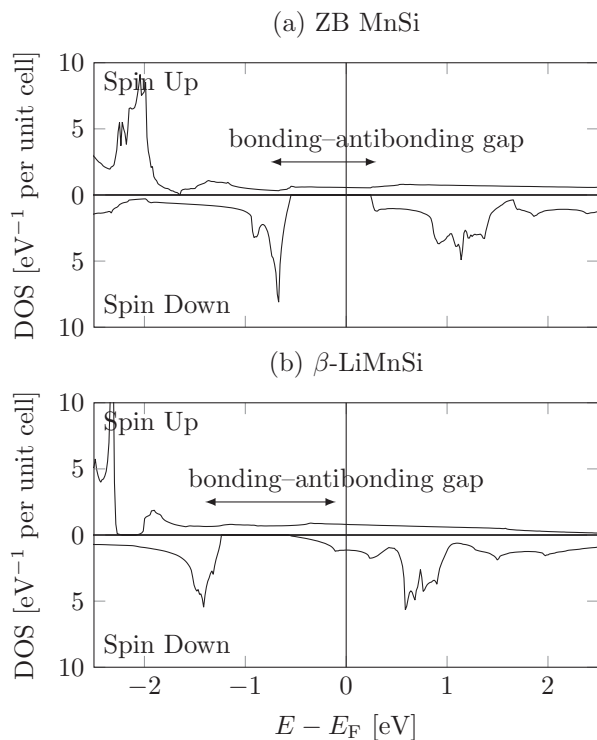


FIG. 2. Density of states for (a) zinc blende MnSi and (b)  $\beta$ -LiMnSi at the optimized lattice constant. Arrow indicates the size of the bonding–antibonding gap at the  $\Gamma$  point.

The pnictides in the  $\beta$ -phase do not have integer magnetic moments and show no gap in either spin channel near  $E_F$ . According to our criteria they are not HMs[28]. Due to the presence of the highly electronegative pnictogen, the Li electron is not completely transferred to the Mn. Instead, the electron from Li causes a reduction in the strength of the d–p hybridization between the pnictogen and the Mn under the tetrahedral environment. With the reduction in the hybridization, the

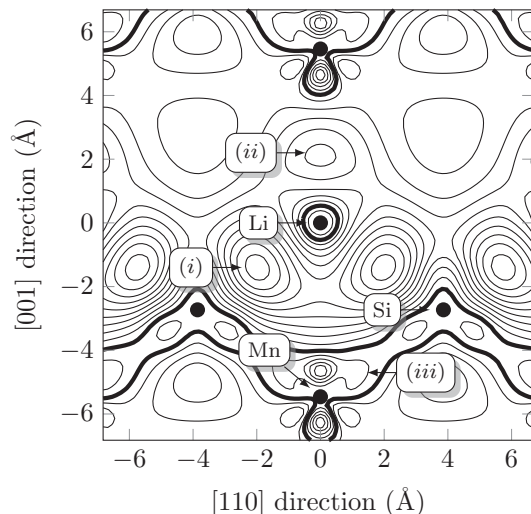


FIG. 3. Contour of the charge density difference ( $\beta$ -LiMnSi minus ZB MnSi) at the same lattice constant. Circles indicate the location of atoms. Labels (i) and (ii) indicates where the Li electron bonds with Si and Mn, respectively, giving a positive contour. Label (iii) shows the area where the bond between Mn and Si weakens and the contour region is negative. The thick black lines indicate the zero contours.

bonding–antibonding gap shrinks and the bottom of the conduction band in the minority spin channel of  $\beta$ -LiMnZ becomes occupied.

### C. Can the three half-Heusler alloys be ferromagnetic or half-metallic?

We are interested in adjusting the lattice constant to force the values of the magnetic moments to be as large as possible. In practice, the consensus is that many devices are thin films and can be grown to match the lattice constants on selected substrates. We can use our results to predict the substrates that match the lattice constants of our compounds with large magnetic moments, but we believe that this will not always be possible for large lattice constants or energies far from equilibrium; therefore, the issue of stability will be addressed later. Tetragonalization can also occur during growth, but it will not necessarily destroy half-metallicity[29]. In Table III, we present detailed ferromagnetic properties of the three compounds in the primitive cells of the three types of structures.

Every alloy in Table III with an integer magnetic moment and a gap is a HM. These include:  $\alpha$ -LiMnN,  $\alpha$ -LiMnP,  $\beta$ -LiMnSi,  $\beta$ -LiMnP, and  $\gamma$ -LiMnSi. The lattice constant can be increased slightly without destroying the half-metallicity since there is a range of lattice constants where  $E_F$  falls within the gap of the semiconducting channel. The magnetic moments of the HMs agree with the predictions of the ionic model plus the contribution of the Li electron to the moment of Mn. The remaining

TABLE III. Summary of the lattice constants, total energies, magnetic moments per unit cell, and energy gaps near the Fermi energy  $E_F$  (with spin channel) of the three compounds in the three phases where the magnetic moment is largest or integer.

Compound	Lattice constant (Å)	Total energy relative to equilibrium $\beta$ (eV)	Magnetic Moment ( $\mu_B/\text{Mn}$ )	Energy gap near $E_F$ (eV)
$\alpha$ -LiMnN	5.300	0.274	5.000	0.819 $\downarrow$
$\beta$ -LiMnN	5.641	1.097	4.990	Metal
$\gamma$ -LiMnN	5.571	2.463	5.000	Metal
$\alpha$ -LiMnP	6.250	0.668	5.000	0.341 $\downarrow$
$\beta$ -LiMnP	6.550	0.944	5.000	1.693 $\downarrow$
$\gamma$ -LiMnP	7.248	3.326	5.000	Metal
$\alpha$ -LiMnSi	6.274	1.384	4.050	Metal
$\beta$ -LiMnSi	6.250	0.318	4.000	0.915 $\downarrow$
$\gamma$ -LiMnSi	6.300	0.392	4.000	0.723 $\downarrow$

alloys are ferromagnets and any change in the lattice constant will decrease the moment. Some of the important features of the individual half-Heusler alloys are discussed below.

In Fig. 4, we show the band structures of  $\beta$ -LiMnSi at two lattice constants: the equilibrium lattice constant and the half-metallic lattice constant. The lowest bands are from the s-orbitals of Si. The next bands, shown in the figures, are the so-called  $t_{2g}$  states triply degenerate states at the  $\Gamma$ -point that split to doubly (upper) and singly (lower) degenerate states as  $\vec{k}$  moves towards X. The next higher energy states at the  $\Gamma$ -point are originally from  $e_g$  states of Mn. Since their lobes point away from nn Si and toward the second neighbor (sn) of the Mn, they do not strongly interact with any other states so they are called the non-bonding states. The half-metallic gap, in Fig. 4(b), is formed between the  $e_g$  states and the doubly degenerate states that split off of the  $t_{2g}$  states. Using the band structure, we can understand why this half-Heusler alloy is not a HM at the equilibrium lattice constant. The  $e_g$  states are insensitive to the separation between nn, but the smaller equilibrium lattice constant causes  $E_F$  to shift up, and intersect with, the  $e_g$  states (Fig. 4(a)) resulting in the disappearance of the half-metallicity.

The reason that  $\alpha$ -LiMnSi is not a HM can be attributed to the fact that Si forms nn pair with Li and sn pair with Mn. The qualitative details are: (i) Ideally, the Li electron can form a covalent bond with Si because the electronegativity of Si is not as large as either P or N. (ii) The sn configuration between Si and Mn favors the p-states of Si to form bonds with three Mn electrons. The bonds are not strong enough to form a gap. Consequently, the TM does not completely transfer its 3 d-electrons to Si and gives a moment of 4.050  $\mu_B$ . The pnictides exhibit half-metallic properties in the

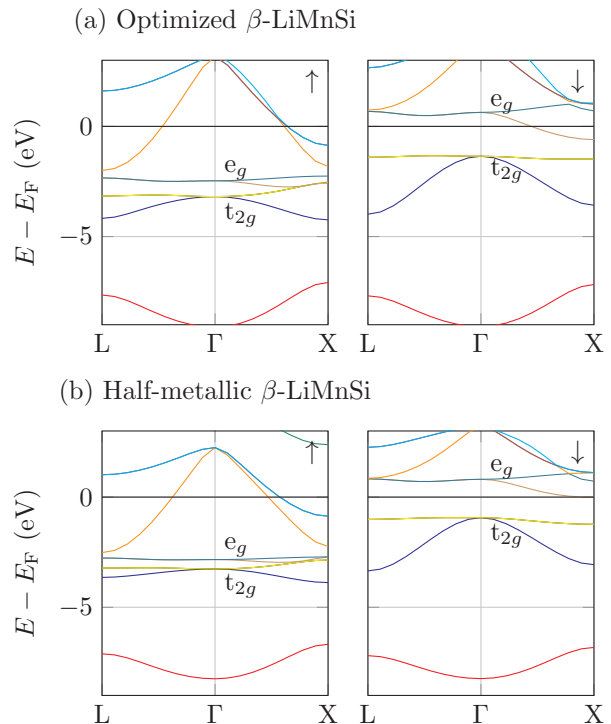


FIG. 4. Band structure for  $\beta$ -LiMnSi along L- $\Gamma$ -X at (a) the equilibrium lattice constant  $a = 5.778$  Å, and (b) the half-metallic lattice constant  $a = 6.250$  Å. The triply degenerate states,  $t_{2g}$ , and the doubly degenerate states,  $e_g$ , near  $E_F$  are labeled.

$\alpha$ -phase at lattice constants larger than their respective equilibrium values. The gap for  $\alpha$ -LiMnP is 0.376 eV while it is 0.696 eV for  $\alpha$ -LiMnN. The gaps reflect the strength of the electronegativity of P with respect to N and the differing lattice constants. The gaps are formed by the  $t_{2g}$  states of Mn and the  $sp^3$  states of the pnictogen, as in the  $\beta$ - and  $\gamma$ -phases, but with a much smaller bonding-antibonding gap.

Next, we focus on the antiferromagnetic cases. In order to investigate this phase, we use the tetragonal cell so that there are two Mn atoms which can have their magnetic moments oriented oppositely. In Table IV, we present the results for the three half-Heusler alloys in the antiferromagnetic phase and their energy difference with respect to the ferromagnetic half-metallic case. From our calculations, all three phases of LiMnSi can be ferromagnetic HMs while LiMnN and LiMnP can be antiferromagnetic HMs at the half-metallic lattice constant, much like LiMnAs[2].

#### D. Can the lithiated alloys in the $\beta$ -phase be more stable than the corresponding compounds in the zinc-blende structure?

We carried out response-function phonon calculations on a  $4 \times 4 \times 4$   $\vec{q}$ -point grid for ZB MnSi at its equilibrium

TABLE IV. Summary of lattice constant and the energy difference between AFM and FM orderings of the three compounds at lattice constants given in Table III. Negative energy differences indicate that the AFM phase is energetically preferred.

Compound	$E_{\text{AFM-EFM}}$ Relative Total Energy (eV)
$\alpha$ -Li <sub>2</sub> Mn <sub>2</sub> N <sub>2</sub>	-0.037
$\beta$ -Li <sub>2</sub> Mn <sub>2</sub> N <sub>2</sub>	-0.292
$\gamma$ -Li <sub>2</sub> Mn <sub>2</sub> N <sub>2</sub>	-0.302
$\alpha$ -Li <sub>2</sub> Mn <sub>2</sub> P <sub>2</sub>	-0.026
$\beta$ -Li <sub>2</sub> Mn <sub>2</sub> P <sub>2</sub>	-0.123
$\gamma$ -Li <sub>2</sub> Mn <sub>2</sub> P <sub>2</sub>	-0.087
$\alpha$ -Li <sub>2</sub> Mn <sub>2</sub> Si <sub>2</sub>	+0.100
$\beta$ -Li <sub>2</sub> Mn <sub>2</sub> Si <sub>2</sub>	+0.347
$\gamma$ -Li <sub>2</sub> Mn <sub>2</sub> Si <sub>2</sub>	+0.324

lattice constant and  $\beta$ -LiMnSi at two lattice constants: its equilibrium value and the lattice constant where the compound is half-metallic. The results are shown in Fig. 5. MnZ in the zinc-blende structure has an unstable transverse acoustic (TA) branch along the zone boundary in the [110] direction ( $\Gamma$ -K). This agrees with the known fact that the ZB structure for MnP-type compounds is not the ground state of these compounds[11].  $\beta$ -LiMnSi, at its equilibrium lattice constant, shows stability in the [110] direction. At the lattice constant that gives half-metallic properties, the six optical branches of  $\beta$ -LiMnSi are also stable. The addition of the Li atom in the structure increases the restoring force against sheer stress.

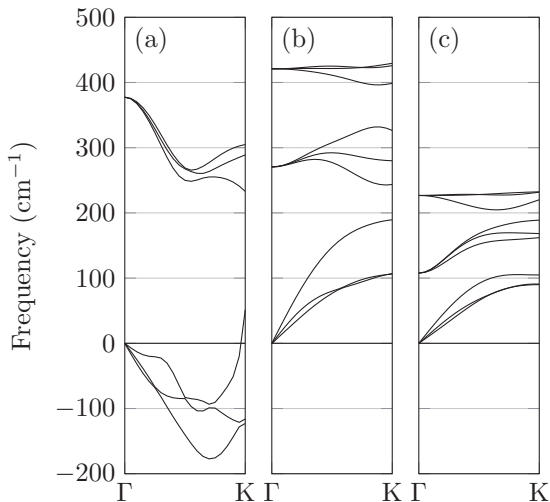


FIG. 5. The phonon bands along  $\Gamma$ -K of (a) zinc blende MnSi, (b)  $\beta$ -LiMnSi at its equilibrium lattice constant  $a = 5.778$  Å and (c)  $\beta$ -LiMnSi at the lattice constant in which it is half-metallic:  $a = 6.590$  Å. Negative values indicate imaginary (unstable) frequencies.

The response-function method allows for the determi-

nation of the phonon bands in the full Brillouin zone. The full-zone phonon bands for  $\beta$ -LiMnSi at the half-metallic lattice constant are provided in Fig. 6

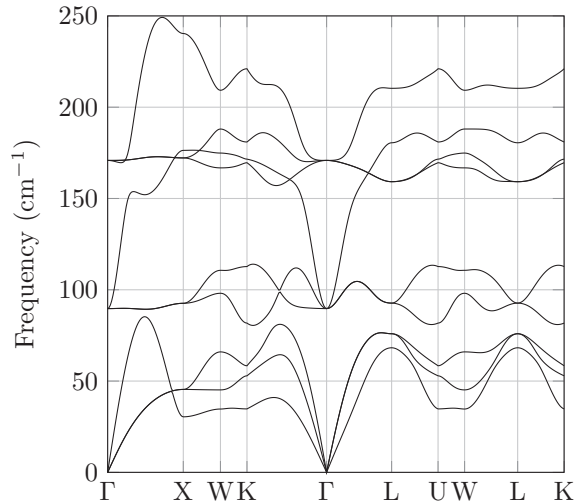


FIG. 6. The full-zone phonon bands of  $\beta$ -LiMnSi at a lattice constant showing half-metallic properties:  $a = 6.590$  Å.

### E. Li<sub>x</sub>MnZ with $x < 1$

Based on the fact that the density of states of  $\gamma$ -LiMnP, given in Fig. 7(a), shows  $E_F$  slightly above the conduction band edge in the minority spin channel, we decided to find new HMs by removing one Li from the conventional cell. The symmetry of the half-Heusler phases allows the removal of any Li atom in the conventional unit cell. The resultant sample is labeled as  $\gamma$ -Li<sub>3</sub>Mn<sub>4</sub>P<sub>4</sub> in the conventional cell or  $\gamma$ -Li<sub>0.75</sub>MnP as an alloy. We anticipated that the removal of a Li atom could lower  $E_F$  into the gap and produce a HM. However, since the Li gave up its electron to other states, an imbalance in the forces drove the atoms, nearest to the vacancy, toward the vacancy and they formed bonds. The resulting compound is not a HM. The bond length between Mn atoms was 4.041 Å before relaxation and 2.452 Å after relaxation. The optimized lattice constant after relaxation is 5.418 Å. The confinement of the spins causes them to anti-align and results in a lower magnetic moment, similar to what we previously found with MnC[30]. The magnetic moment of  $\gamma$ -Li<sub>3</sub>Mn<sub>4</sub>P<sub>4</sub> reduces to 1.145  $\mu_B$  per Mn atom.

### F. Modified Slater-Pauling Rule

The lithiated half-Heusler alloys either have 13 or 12 valence electrons per unit cell. Since the total number of valence electrons  $N$  is smaller in these alloys than in the TM-related compounds, the modified SP rule should definitely be modified. The band structure of  $\beta$ -LiMnSi

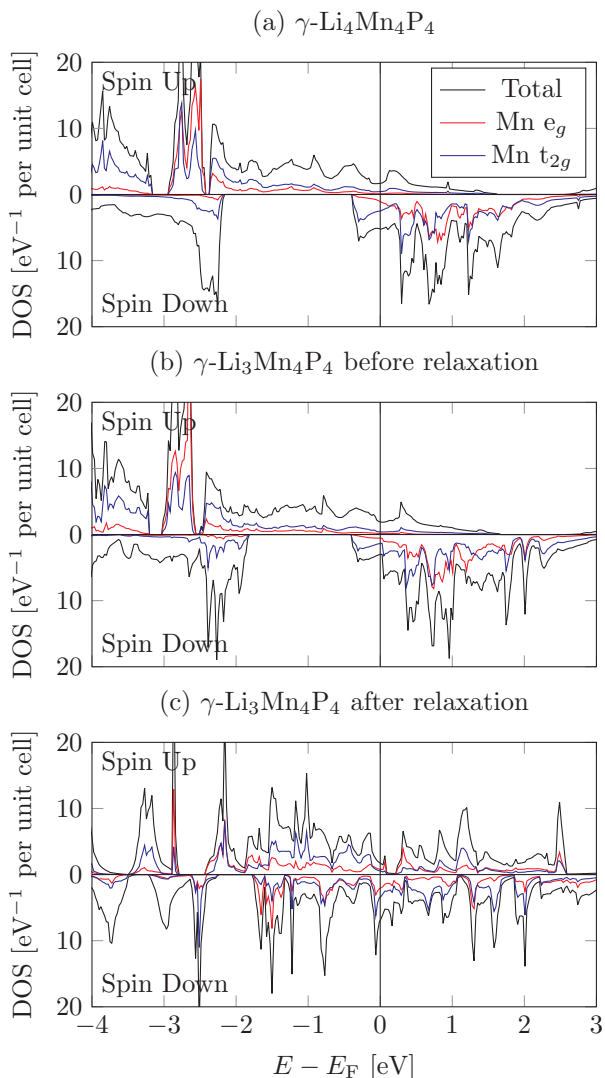


FIG. 7. DOS for (a)  $\text{Li}_4\text{Mn}_4\text{P}_4$ , (b)  $\text{Li}_3\text{Mn}_4\text{P}_4$  before relaxation and (c)  $\text{Li}_3\text{Mn}_4\text{P}_4$  after cell and ion relaxation. Shaded regions show the partial DOS for the  $e_g$  and  $t_{2g}$  states around the Mn atoms.

in the primitive cell, shown in Fig. 4(b), shows four bands in the semiconducting channel, so  $N_{\downarrow} = 4$ . From Eq. 1, the modified SP rule is

$$M = (N - 8)\mu_B, \quad (2)$$

so for  $\text{LiMnSi}$ ,  $N = 12$  and  $M$  is  $4 \mu_B$  per formula unit. Similarly,  $M$  is  $5 \mu_B$  per formula unit for the pnictides. The calculated moments in Table III agree well to the predicted results of Eq. 2, however the modified SP rule is not able to account for the antiferromagnetism in the cases where  $Z$  is a pnictogen.

#### IV. SUMMARY

The fact that Li easily gives up its electron to Mn led us to investigate three Li-based half-Heusler alloys, each involving one TM element per formula, for the possibility of them being ferromagnetic with large magnetic moments. Three different arrangements of the atoms inside a unit cell, denoted  $\alpha$ -,  $\beta$ - and  $\gamma$ -phases, appear in the literature. We offer a unified view of bonding in the three alloys based on previous studies on TM-related half-Heusler alloys involving two TMEs[9]. The strongest bond is formed between the  $Z$  and Mn resulting in the primary bonding-antibonding gap. To understand the role played by the Li, we compared the bonding properties of  $\beta$ - $\text{LiMnSi}$ , a prototype, to  $\text{MnSi}$ , a HM in zinc blende structure. Using the tetragonal cell, we found that  $\alpha$ - $\text{LiMnP}$ ,  $\alpha$ - $\text{LiMnN}$  and  $\beta$ - $\text{LiMnP}$  are antiferromagnetic while  $\text{LiMnSi}$  is a ferromagnetic HM in the  $\beta$  and  $\gamma$  phases. The reasons for the above facts are provided. The magnetic moments for the ferromagnetic alloys are all larger than  $3 \mu_B$  per formula unit. These alloys should be good candidates as spintronic materials for devices operating at or above room temperature. A new modified SP rule predicting the magnetic moments in this class of half-Heusler alloys is proposed and predicts well for the three alloys with half-metallic properties, however the rule is incapable of predicting antiferromagnetism. The stability against shear stress, as compared to the simple ZB structure, is demonstrated by calculating the phonon spectrum, [110] direction of the Brillouin zone, using the response function scheme. We show that  $\text{MnP}$  is unstable along the [110] direction and find that the half metallic Li-based alloys can be stable. Finally, we show that the removal of Li atoms will not lower  $E_F$  into the gap region as we originally believed. Instead, the atoms surrounding the vacancy left by the Li will relax towards the opening, bond, and then destroy the half-metallicity. Hopefully, these results will facilitate the search and subsequent growth of new HMs involving alkali or even alkaline metals.

- [1] D. Kieven, R. Klenk, S. Naghavi, C. Felser, and T. Gruhn, *Physical Review B* **81**, 075208 (2010).  
 [2] T. Jungwirth, V. Novák, X. Martí, M. Cukr, F. Máca, A. B. Shick, J. Mašek, P. Horodyská, P. Němec, V. Holý, J. Zemek, P. Kužel, I. Němec, B. L. Gallagher, R. P. Campion, C. T. Foxon, and J. Wunderlich, *Physical Re-*

- view B* **83**, 035321 (2011).  
 [3] P. Larson, S. D. Mahanti, and M. G. Kanatzidis, *Physical Review B* **62**, 12754 (2000).  
 [4] F. B. Mancoff, J. F. Bobo, O. E. Richter, K. Bessho, P. R. Johnson, R. Sinclair, W. D. Nix, R. White, and B. M. Clemens, *J. Materi. Res.* **14**, 1560 (1999).

- [5] R. A. de Groot, F. M. Mueller, P. G. van Engen, and K. H. J. Buschow, *Physical Review Letters* **50**, 2024 (1983).
- [6] I. Galanakis, P. Mavropoulos, and P. H. Dederichs, *Journal of Physics D: Applied Physics* **39**, 765 (2006).
- [7] J. Tobola and J. Pierre, *Journal of Alloys and Compounds* **296**, 243 (2000).
- [8] R. W. G. Wyckoff, *Crystal Structures*, 2nd ed., Vol. 1 (John Wiley & Sons, 1963).
- [9] M. Shauhgnessy, L. J. Damewood, C. Y. Fong, L. H. Yang, and C. Felser, *Journal of Applied Physics* **113**, 043709 (2013).
- [10] K. Schwarz, *Journal of Physics F: Metal Physics* **16**, L211 (1986).
- [11] H. Akinaga, T. Manago, and M. Shirai, *Journal of Applied Physics* **39**, L1118 (2000).
- [12] J. E. Pask, L. H. Yang, C. Y. Fong, W. E. Pickett, and S. Dag, *Physical Review B* **67**, 224420 (2003).
- [13] J. Kübler, *Physica B+C* **127**, 257 (1984).
- [14] S. Baroni, S. de Gironcoli, A. Dal Corso, and P. Gianozzi, *Reviews of Modern Physics* **73**, 515 (2001).
- [15] G. Kresse and J. Furthmüller, *Physical Review B* **54**, 11169 (1996).
- [16] G. Kresse and J. Furthmüller, *Computational Materials Science* **6**, 15 (1996).
- [17] G. Kresse and J. Hafner, *Physical Review B* **49**, 14251 (1994).
- [18] G. Kresse and J. Hafner, *Physical Review B* **47**, 558 (1993).
- [19] P. Hohenberg and W. Kohn, *Physical Review* **136**, B864 (1964).
- [20] J. P. Perdew, K. Burke, and M. Ernzerhof, *Physical Review Letters* **77**, 3865 (1996).
- [21] L. J. Damewood and C. Y. Fong, *Physical Review B* **83**, 113102 (2011).
- [22] L. Chioncel, E. Arrighoni, M. I. Katsnelson, and A. I. Liechtenstein, *Physical Review Letters* **96**, 137203 (2006).
- [23] P. E. Blöchl, *Physical Review B* **50**, 17953 (1994).
- [24] H. J. Monkhorst and J. D. Pack, *Physical Review B* **13**, 5188 (1976).
- [25] X. Gonze, B. Amadon, P. M. Anglade, J. M. Beuken, F. Bottin, P. Boulanger, F. Bruneval, D. Caliste, R. Caracas, M. Côté, T. Deutsch, L. Genovese, P. Ghosez, M. Giantomassi, S. Goedecker, D. R. Hamann, P. Hermet, F. Jollet, G. Jomard, S. Leroux, M. Mancini, S. Mazevet, M. J. T. Oliveira, G. Onida, Y. Pouillon, T. Rangel, G. M. Rignanese, D. Sangalli, R. Shaltaf, M. Torrent, M. Verstraete, G. Zérah, and J. W. Zwanziger, *Comput. Phys. Commun.* **180**, 2582 (2009).
- [26] X. Gonze, G. M. Rignanese, M. Verstraete, J. M. Beuken, Y. Pouillon, R. Caracas, F. Jollet, M. Torrent, G. Zérah, M. Mikami, P. Ghosez, M. Veithen, J. Y. Raty, V. Olevano, F. Bruneval, L. Reining, R. W. Godby, G. Onida, D. R. Hamann, and D. Allan, *Z. Physik* **220**, 558 (2005).
- [27] W. M. Haynes, ed., *CRC Handbook of Chemistry and Physics*, 93rd ed. (CRC Press/Taylor and Francis, Boca Raton, FL, 2013).
- [28] C. Y. Fong, M. C. Qian, K. Liu, and L. H. Yang, *Journal of Nanoscience and Nanotechnology* **8**, 3652 (2008).
- [29] K. Özdoğan, E. Şaşıoğlu, and I. Galanakis, *Journal of Applied Physics* **111**, 113918 (2012).
- [30] M. C. Qian, C. Y. Fong, W. E. Pickett, and H.-Y. Wang, *Journal of Applied Physics* **95**, 7459 (2004).

#### ACKNOWLEDGMENTS

Work at UC Davis was supported in part by the National Science Foundation Grant No. ECCS-0725902. Work at Lawrence Livermore National Laboratory was performed under the auspices of the U.S. Department of Energy by Lawrence Livermore National Laboratory under Contract DE-AC52-07NA27344. One of the authors (L. D.) would like to thank Barry Klein for useful discussions.”